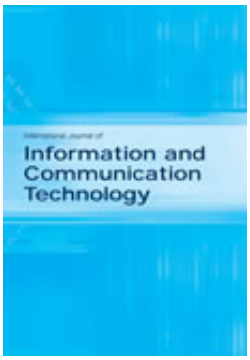

International Journal of Information and Communication Technology

ISSN online: 1741-8070 - ISSN print: 1466-6642
https://www.inderscience.com/ijict

Performance optimisation of prefabricated concrete structure using intelligent finite element analysis

Jie Gao

DOI: 10.1504/IJICT.2026.10075880

Article History:

Received:	23 September 2025
Last revised:	28 October 2025
Accepted:	29 October 2025
Published online:	02 February 2026

Performance optimisation of prefabricated concrete structure using intelligent finite element analysis

Jie Gao

School of Engineering Management,
Anhui Audit Vocational College,
Hefei, 230000 China
Email: JieGaoo@outlook.com

Abstract: Driven by rapid urbanisation and 'dual-carbon' targets, conventional cast-in-place construction struggles with high energy use, pollution, and low efficiency. Prefabricated concrete buildings improve productivity and sustainability, yet joint connections govern global load capacity, seismic behaviour, and durability. This study develops and validates a finite-element optimisation framework for prefabricated concrete joints. Concrete is modelled with the concrete damage plasticity (CDP) formulation and steel components with the von Mises yield criterion, including nonlinear material behaviour, contact interaction, and displacement-controlled loading (perfect bond assumed between sleeve grout and reinforcement). Parametric analyses evaluate concrete strength (C30/C40/C50), reinforcement ratio (1.0%/1.2%/1.5%), and bolt diameter (18/20/25 mm). Relative to C30, bearing capacity increases by 4.53% (C40) and 9.93% (C50); raising reinforcement to 1.2% and 1.5% improves capacity by 6.04% and 15.29%; and enlarging bolts to 20 and 25 mm increases capacity by 6.15% and 13.34%. Validation achieves 6%–8% average error and $R^2 = 0.984$.

Keywords: intelligent construction; prefabricated concrete structure; node mechanical performance; finite element analysis; structural optimisation.

Reference to this paper should be made as follows: Gao, J. (2026) 'Performance optimisation of prefabricated concrete structure using intelligent finite element analysis', *Int. J. Information and Communication Technology*, Vol. 27, No. 2, pp.19–40.

Biographical notes: Jie Gao obtained her Bachelor's in Engineering Management from Anhui Institute of Architecture and Civil Engineering (now Anhui University of Architecture) in 2007, and Master's in Architectural and Civil Engineering from Guilin University of Technology in 2012. She is currently an Associate Professor at the School of Engineering Management, Anhui Audit Vocational College. Her research directions include engineering management and engineering cost estimation.

1 Introduction

Traditional construction methods often come with problems such as long construction periods, severe resource waste, and difficulty in controlling construction quality while meeting the growing demand for construction. In order to address these challenges, the construction industry has begun to explore new building methods, among which

prefabricated building technology has emerged as an important innovation in the modern construction industry. Prefabricated buildings, through standardised production processes and precise component manufacturing, can significantly reduce the complexity and time of on-site construction, greatly shortening the construction period of building projects. Due to the components being produced in a factory environment, their manufacturing process can strictly control quality, reducing waste and pollution on the construction site.

Prefabricated concrete structure nodes refer to the parts that combine different prefabricated components through connectors, fixings, or other connection methods. There are usually various connection methods for nodes, including bolt connections, welding, plug-in connections, etc. (Magar, 2020). The design of structural nodes directly determines the performance of prefabricated concrete structures, including their bearing capacity, deformation capacity, seismic performance, and other aspects. The construction mode of prefabricated buildings requires nodes to have good adaptability, ensuring the accuracy and quality of components during the factory prefabrication process and ensuring good connection performance during on-site assembly. Suppose the node design is improper or there are defects in the node connection method. In that case, it may lead to the fragility of the entire structural system, thereby affecting the safety and durability of the building (Holly and Abrahoim, 2020). Traditional prefabricated structural nodes are often connected using steel mesh or steel bar connections, which can meet basic connection requirements. However, due to the complex stress distribution at the node location, differences in material properties, and potential errors during construction, these traditional nodes often suffer from problems such as local stress concentration and insufficiently tight connections (Zhong et al., 2019). Through intelligent construction technology, components of prefabricated concrete structures can be designed through precise modelling and simulation and produced and inspected accurately during the manufacturing phase. In addition, intelligent construction technology can also monitor every step of the construction process in real time, ensuring that the assembly and connection of each component meet the design requirements and minimising human errors and quality issues (Shi et al., 2022). The application of these technologies enables more precise control over the node design and construction process of prefabricated concrete structures, which helps to improve the mechanical performance of nodes and the overall safety of the structure (Luo et al., 2025).

This article aims to perform a comprehensive investigation into the mechanical properties of nodes within prefabricated concrete structures, investigating methods to enhance seismic performance and bearing capacity and durability of nodes through optimisation of node design. Through the optimisation analysis of this study, the aim is to provide a new technological path for the development of prefabricated building technology and theoretical support for the widespread application of prefabricated concrete structures. Especially in the context of intelligent construction, this research aims to advance the intelligent and sustainable developments in building structures, while also improving the practical application of prefabricated buildings in engineering contexts.

Despite the increasing adoption of prefabricated concrete systems, most existing studies focus on general component performance rather than the mechanical optimisation of connection nodes under intelligent construction workflows. Furthermore, the integration between numerical modelling, digital fabrication, and on-site assembly validation remains insufficiently explored, leading to a research gap in the closed-loop linkage between simulation and implementation.

To address these limitations, this study makes the following three main contributions:

1 It establishes a validated finite element modelling framework for prefabricated concrete joints based on the concrete damage plasticity (CDP) model, incorporating material nonlinearity, contact, and preload effects.

2 It develops a multi-parameter optimisation and sensitivity evaluation approach that quantifies the effects of reinforcement ratio, concrete strength, and bolt diameter on mechanical performance, producing simplified empirical design formulas.

3 It proposes a simulation-to-manufacture integration workflow, linking finite element optimisation, BIM/digital twin modelling, and sensor-based monitoring, forming a replicable digital framework for intelligent construction.

These contributions collectively close the gap between numerical analysis and practical intelligent prefabrication, enhancing both theoretical understanding and engineering applicability.

2 Mechanical analysis of prefabricated concrete structure nodes

Building upon the background established in the Introduction, this section analyses the fundamental mechanical behaviour of prefabricated concrete structure nodes, forming the theoretical basis for subsequent finite element modelling. The identified mechanical characteristics and common issues of prefabricated nodes provide the key parameters and boundary conditions for the finite element simulation discussed in the next section.

The mechanical characteristics of prefabricated concrete structures are significantly influenced by the method of splicing employed, and steel bar connection forms between prefabricated components (Chang et al., 2023). The common forms of nodes include wall panel nodes and beam slab column nodes, which bear the main loads in the structure. Therefore, their design and construction quality are crucial to the mechanical performance of the structure.

According to the different mechanical properties, the nodes of prefabricated concrete structures can be divided into rigid nodes and semi-rigid nodes (Guo et al., 2021). Rigid nodes have high connection strength and stiffness and can effectively transmit loads between components. They are usually used in situations that require high mechanical performance. Semi-rigid nodes are relatively flexible and can adapt to deformation between components within a certain range. They are usually used in less demanding application environments (Yu et al., 2022). The choice of node type and steel bar connection method depends on the design requirements, construction conditions, and mechanical performance requirements of the structure.

2.1 Analysis of the advantages of prefabricated concrete structures

1 The factory production of prefabricated components not only ensures the consistency of component quality but also completes the production of a large number of components in a short period, saving time and cost on the construction site. Due to the use of mechanised and automated equipment in the production process, errors and uncertainties in manual operations have been reduced, enhancing the precision and effectiveness of production processes (Liu et al., 2021b).

2 The utilisation of prefabricated components has the potential to significantly reduce the duration of construction projects and enhance the overall pace of construction activities. It not only avoids the complex process of on-site concrete pouring but also saves a lot of time and manpower investment in concrete mixing, transportation, pouring, and maintenance. Moreover, it greatly reduces the on-site concrete curing time and the time for formwork support and removal, avoiding the impact of weather and other factors on the construction progress (Jiang et al., 2019). For example, in the cold winter, traditional cast-in-place concrete construction faces cooling and curing problems, while prefabricated components can still be produced and constructed smoothly, thus avoiding winter construction stagnation and saving much later work.

3 By adopting mechanised production, standardised processes, and strict quality control in factories, the quality of precast concrete components is usually better than those poured on site. This not only improves the overall quality of the components but also reduces maintenance and replacement costs in the later stages (Xie et al., 2020). Producing under unified standards in the factory can effectively avoid common quality problems such as honeycomb and rough surfaces during on-site construction. The maintenance conditions can be strictly controlled, and the production environment can adjust temperature and humidity to reduce the impact of weather changes on component quality.

4 In the construction of prefabricated structures, the process of concrete vibration is effectively transferred to the factory to reduce noise pollution, and the production process is more refined, reducing waste during the construction process (Zhang and Li, 2021). In the process of factory production, the generation of waste has been effectively controlled, and the waste generated during the production process can be recycled, further reducing the pollution of waste to the environment.

2.2 Mechanical performance analysis of assembled concrete structure nodes

2.2.1 Bearing capacity characteristics

The bearing capacity of prefabricated concrete structure nodes is their most fundamental mechanical performance, mainly including axial compression, bending resistance, and shear resistance (Fang et al., 2022).

1 The axial pressure of nodes connected by sleeve grouting or mechanical connection is mainly transmitted through the gripping effect between grouting material and steel bars or the interlocking of mechanical components (Ding et al., 2019). If there are defects in the connection interface, such as insufficient grouting or inadequate reinforcement anchoring, it can easily lead to stress concentration and a decrease in bearing capacity (Elsayed and Nehdi, 2017).

2 The setting of interface roughness and shear-resistant steel bars can effectively improve the bending resistance, but if the interface is not treated properly, shear slip is prone to occur, resulting in a decrease in bending stiffness (Tullini and Minghini, 2016).

3 The local shear resistance structure of the node region is crucial for preventing shear failure (Pang and Li, 2024).

2.2.2 Stiffness and deformation characteristics

The stiffness of nodes directly affects the deformation capacity of structures under load, and its characteristics manifest as periodic degradation (Han et al., 2024). In the elastic stage, the node maintains a high stiffness under the initial load, and the deformation is linearly related to the load. At this time, there is no significant damage to the connection part. When the load exceeds the critical value, cracks appear in the concrete or connection interface of the node area, the stiffness significantly decreases, and the deformation rate accelerates. After entering plastic deformation, the node absorbs energy through the yielding of steel bars or plastic deformation of connectors, further reducing stiffness but significantly improving deformation capacity (Birkner et al., 2024).

2.2.3 Durability and resistance to continuous collapse

Concrete creep, shrinkage, and changes in environmental temperature and humidity can cause stress redistribution in the node area, leading to joint opening or closing and affecting long-term stability. This effect can be alleviated by reserving deformation joints or using flexible sealing materials (Criel et al., 2015). The node needs to have a certain residual bearing capacity and maintain overall stability through the catenary effect (tension of the tensioned steel bars) after local component failure, with the ability to resist continuous collapse (Valipour and Khayat, 2018).

2.3 Common problems of prefabricated concrete structure nodes

Due to the complexity of construction, differences in materials, and special construction techniques, problems such as crack propagation and insufficient strength often occur at node locations.

1 The material shrinkage effect, sudden changes in node geometry leading to local stress concentration, interface bonding failure, and fatigue damage accumulation during the hardening process of concrete can all cause crack propagation problems at node locations (Liu et al., 2021a).

2 Prefabricated nodes rely on connectors such as sleeves, bolts, etc., to achieve internal force transmission. If the structural design does not form a coherent force flow transmission path, it will lead to abnormal stress distribution. Unreasonable structural design, such as insufficient anchorage length or defective reinforcement configuration, can lead to insufficient stress strength of nodes.

3 If there are errors during the construction process, such as insufficient grouting density, deviation in component installation, etc., it will lead to stress concentration and reduce the bending bearing capacity (Kallel et al., 2023).

4 The connection nodes between components are particularly critical to the integrity of prefabricated concrete structures. Suppose the bearing capacity, connection method, and joint treatment of these nodes are not fully considered in the design and construction. In that case, the reliability of the nodes may be affected, directly leading to a decrease in the overall performance of the structure (Wenke and Dolan, 2021). Improper node design or ineffective treatment of joint interfaces in prefabricated components can easily make nodes weak links. When buildings

encounter disasters such as earthquakes, these weak nodes become key points of structural damage (Ma et al., 2024).

3 Finite element analysis of prefabricated concrete structure nodes

Based on the mechanical understanding from the previous section, the following finite element analysis is conducted to numerically evaluate and reproduce the node behaviour under axial compression. The simulation results not only validate the experimental findings but also set the foundation for subsequent parameter optimisation and design improvement presented in Section 4.

3.1 Node construction and model

This study focuses on a prefabricated concrete building project, specifically examining the column connection nodes within the frame structure, including the central region of the nodes and the prefabricated concrete columns, forming a symmetrical structure above and below. The core area of the node is composed of a 10 mm thick grouting sleeve, a 20 mm thick Q345 steel plate, and a 10.9-grade high-strength bolt with a diameter of 20 mm. The grouting sleeve material is Q355 steel. The length of the test column is selected as 3,500 mm, the cross-sectional size is 200 mm × 400 mm, the steel reinforcement is HRB400 steel, and the concrete is C30 concrete.

The reinforcement and dimensions of the node structure are shown in Figure 1, and the measured mechanical properties of steel bars and other materials are shown in Table 1.

Table 1 Actual measured values of mechanical properties of steel

Material category	*Elastic modulus (E_0/Mpa)*	*Yield strength (f_y/Mpa)*	*Ultimate strength (f_{cu}/MPa)*
HRB400(A10)	2.00×10^5	408	549
HRB400(A18)	2.00×10^5	417	566
Q345 (20 mm thick)	2.01×10^5	335	517
Q355 (10 mm thick)	2.02×10^5	365	484
10.9 grade high-strength bolt (20 mm)	2.06×10^5	900	1,000

The permissible dimensional tolerance for each steel specimen was within ±1.0 mm in diameter and ±2.0 mm in length. The actual measured yield and ultimate strengths showed a normal distribution with standard deviations of 3.5% and 4.2%, respectively, across five tested batches. The coefficient of variation (COV) remained below 5%, indicating acceptable batch consistency and ensuring comparability of mechanical properties across all specimens. The steel materials used in this study conform to the following standards and typical mechanical property ranges:

- Q345 steel: GB/T 1591–2018 ‘high strength low alloy structural steels’, with yield strength of 345 MPa (range: 315–390 MPa) and ultimate strength of 470–630 MPa.

- Q355 steel: GB/T 1591–2018, with yield strength of 355 MPa (range: 335–390 MPa) and ultimate strength of 470–630 MPa, equivalent to EN 10025-2 S355 or ASTM A572 Grade 50.
- HRB400 reinforcing steel: GB/T 1499.2–2018 ‘steel for reinforced concrete – part 2: hot rolled ribbed bars’, with yield strength of 400 MPa (range: 360–440 MPa) and ultimate strength of 540–670 MPa.
- 10.9-grade high-strength bolts: GB/T 3098.1–2010 ‘mechanical properties of fasteners’, with yield strength approximately 900 MPa and ultimate strength 1,000–1,040 MPa, consistent with ISO 898-1:2013.

These standards ensure that the experimental and numerical results are based on representative and traceable material properties, allowing direct comparison with international design codes and empirical models.

Figure 1 Node construction reinforcement and size (mm), (a) schematic diagram of prefabricated column nodes (b) column section diagram

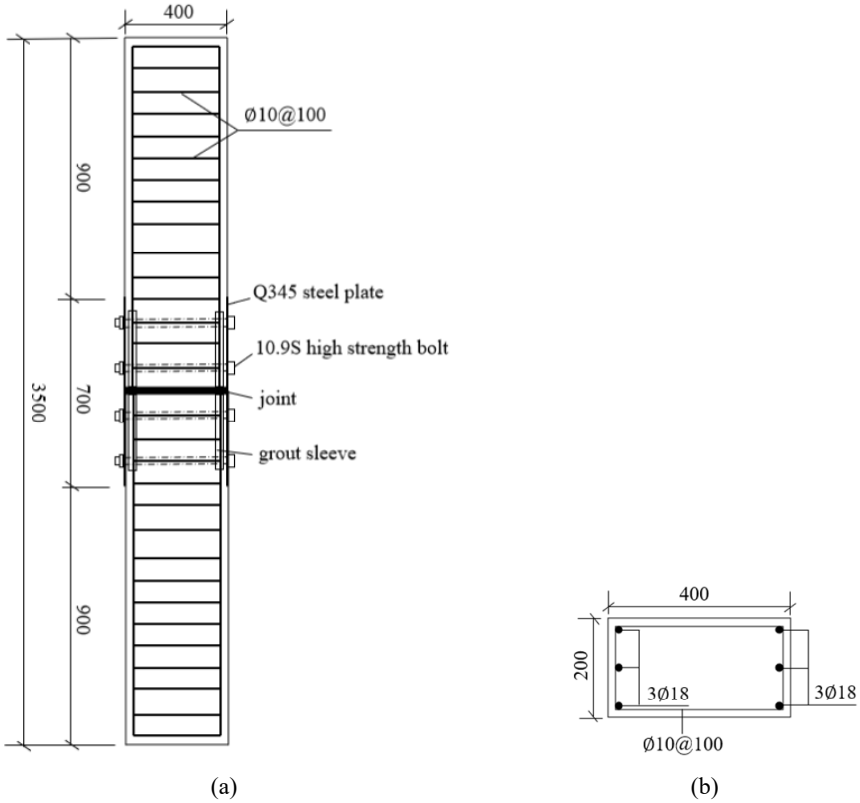

(a) (b)

This study is primarily applicable to prefabricated beam-column joints and column-column compression nodes connected through grouted sleeve and bolted assemblies, following a top-down on-site assembly sequence typical of frame structures. The conclusions and optimisation strategies are directly transferable to axially loaded, compression-dominated connections under monotonic or quasi-static loading conditions.

However, the findings are not directly applicable to joint configurations governed by combined bending–shear interactions, cyclic or seismic excitation, or connections using post-tensioned tendons or dry-insert mechanisms, where different load paths and failure modes prevail. For these cases, additional verification involving dynamic loading protocols and energy dissipation analysis is necessary before adoption. This clarification defines the practical engineering boundaries of the proposed framework and supports external validity by delineating where the model can be confidently extended to field applications.

3.2 Analysis of node test results

3.2.1 Bearing capacity analysis

The experimental findings presented in Figure 2 indicate that the incorporation of metal plates on either side of the concrete column substantially influences the structural and mechanical behaviour of the column under axial loading. The bidirectional constraint mechanism formed by the contact interface between steel plate and concrete during load transfer changes the stress distribution pattern of traditional concrete components. When the axial load continues to increase to the yield stage of the material, the transverse compression effect of the metal sheet begins to dominate the stress state in the contact area. This contact mechanical behaviour between heterogeneous materials leads to two key mechanical phenomena: firstly, the formation of a three-dimensional complex stress field under compression in the interface area, causing irreversible damage accumulation in the microstructure of concrete; Secondly, due to the differences in deformation coordination of heterogeneous materials, significant stress gradients are generated near the contact surface, resulting in the degradation of the mechanical properties of the effective load-bearing section of the structure.

Figure 2 Deflection load curve (see online version for colours)

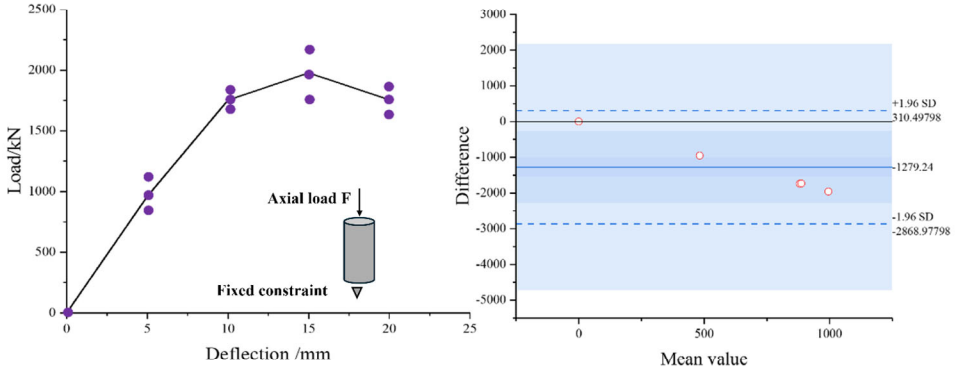

The observed mechanical phenomena in the experiment reveal the intrinsic mechanism of heterogeneous material composite structures. In the process of load transfer, metal sheets do not simply exist as reinforcing components, but their composite interaction system with the concrete matrix essentially changes the failure mode of the structure. This change is mainly reflected in two aspects: firstly, the transformation of the failure mode from the traditional longitudinal splitting failure to the composite failure of interface

delamination accompanied by local crushing; Secondly, there is a change in the degradation path of bearing capacity, where the structure no longer exhibits brittle failure characteristics of a single material, but rather shows a phased and multi-level progressive failure process.

3.2.2 Analysis of collaborative force between steel plate and reinforcement

From Figure 3, the strain of the longitudinal reinforcement and steel plate of the specimen under load can be obtained. The steel plate connected to the tensile steel plate of the specimen always remains in the elastic stage, which reflects the weak deformation ability of the steel plate and the inability to exert the synergistic effect with the longitudinal reinforcement fully. The main reason is the relative slip between the steel plate and the specimen, which leads to the steel plate not effectively working together with the concrete and longitudinal reinforcement, thereby weakening the overall load-bearing capacity of the structure. This slip effect is a key factor in the failure of the steel plate to reach its yield strength, and also the reason for the insufficient bearing capacity of the specimen. Therefore, when optimising the design, it is necessary to consider the interaction between steel plates, steel bars, and concrete to avoid slip phenomena and enhance the structural stability and load-bearing capacity.

Figure 3 Load steel strain diagram (see online version for colours)

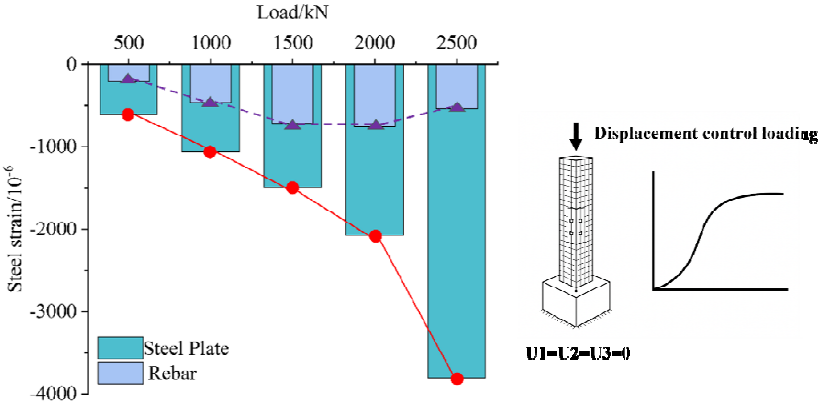

3.3 Finite element analysis

In this study, the CDP model was adopted to simulate the nonlinear behaviour of concrete, considering both compressive crushing and tensile cracking mechanisms. Key parameters were set as follows: dilation angle = 36°, flow potential eccentricity = 0.1, K_c = 0.667, viscosity parameter = 0.0005 and the ratio of initial biaxial to uniaxial compressive yield stress = 1.16. These parameters were determined based on recommendations in the ABAQUS material library and calibrated through comparison with experimental stress-strain data from material tests on the C30 concrete used in the specimen. The tensile and compressive damage evolution curves were defined per empirical relations in GB 50010-2010 and further refined to match the observed load–displacement behaviour in Section 3.2. The Willam-Warnke failure surface was also used

for validation, and results indicated that the CDP model provided better convergence and closer agreement with experimental results.

In addition, the von Mises yield criterion was adopted for all metallic materials (reinforcing steel, plates, and bolts), assuming isotropic hardening with a bilinear stress-strain relation. The strain-hardening modulus was defined as 2% of the elastic modulus to reflect the post-yield behaviour observed in coupon tests. For high-strength bolts (grade 10.9), an equivalent elasto-plastic connector element was introduced to represent the shank–nut assembly. A preload force corresponding to 70% of the nominal yield strength was applied to simulate the tightening condition. The bolt–hole contact was modelled using a surface-to-surface interaction with a hard-contact normal behaviour and a tangential friction coefficient of $\mu = 0.2$, allowing for limited slip but preventing penetration. This treatment ensured realistic transfer of shear and clamping forces during the loading process.

Furthermore, the bond-slip behaviour between the grouted sleeve and the reinforcing bar was not explicitly modelled using nonlinear interface elements due to the absence of detailed experimental data. Instead, a perfect bond assumption was adopted, representing a fully anchored condition between the sleeve grout and rebar. This simplification is consistent with prior research and the provisions of ACI 408R-03 and GB 50010–2010, which indicate that properly grouted sleeves generally achieve sufficient bond capacity before bar yielding. However, it should be noted that this assumption may lead to a slightly overestimated stiffness and ultimate load capacity, as the potential local slip and progressive debonding effects are neglected. Consequently, the direction of bias is conservative in deformation prediction but optimistic in strength estimation.

In the finite element model, different element types were selected according to material characteristics: the concrete components were modelled using three-dimensional solid elements (C3D8R) to capture the nonlinear stress distribution, the steel plates and bolts were modelled using solid elements, and the reinforcement was represented by beam elements (B31) with perfect bonding to concrete. A refined mesh generation strategy was adopted, with average element sizes of 10 mm, 15 mm, and 20 mm applied sequentially to perform a **mesh independence study. The results showed that the variation in ultimate load was less than 2.5% between the 10 mm and 15 mm meshes, indicating convergence. The computational cost increased from 2.1 h to 3.9 h as the mesh was refined, and convergence criteria were defined by force and displacement residuals below 1×10^{-3}. Therefore, the 15 mm mesh size was selected as the optimal balance between accuracy and efficiency.

In the finite element model, the boundary conditions were defined by fully restraining the bottom surface of the column base to simulate a fixed support, while the upper end was subjected to vertical loading. The loading was applied in a displacement-controlled manner to ensure stable convergence near the peak load. The loading rate was maintained at 0.5 mm/min to capture the nonlinear deformation behaviour accurately. For contact settings, a surface-to-surface contact was established between the steel plate and the concrete surface, with a steel-concrete friction coefficient of 0.3, allowing for limited separation and slip during loading. These conditions were designed to replicate realistic interaction behaviour between steel and concrete interfaces under compressive loading.

Moreover, to enhance the quantitative validation of the numerical model, additional comparisons of crack and crushing patterns, as well as strain and stress distributions at critical sections, were conducted. The simulated crack initiation and propagation zones in the concrete core were found to closely correspond to the experimentally observed

cracking regions, particularly around the interface between the grouted sleeve and adjacent concrete, and at the tensile edge of the column. The CDP model successfully reproduced the concrete crushing zone near the compression face of the node core, consistent with test observations. The strain contours of longitudinal reinforcement and stress distribution in the steel plates along the joint centreline matched well with measured data, showing a deviation within 8% in peak strain and 6% in stress magnitude. These results demonstrate the model's capability to capture not only global load-displacement behaviour but also localised damage evolution, providing a strong quantitative basis for the model's predictive reliability and physical credibility.

3.3.1 Load axial displacement analysis

As illustrated in Figure 4, it is evident that during the preliminary phase of structural stress, when the longitudinal steel bars have not yet entered the yielding state, the agreement between the experimental data and the simulated curve is high. This suggests that the developed numerical model is capable of accurately representing the stiffness characteristics and deformation behaviours of the specimen during the elastic phase. As the load continues to increase to the critical point of steel yield, the difference between experimental phenomena and simulation results gradually becomes apparent. The maximum load of the test column reached 2,195.22 kN, and after reaching the peak load, it showed a sharp decline in bearing capacity; this phenomenon can be primarily attributed to the brittle failure mode exhibited by the specimen during the testing procedure. Due to the sudden crushing of concrete materials or instantaneous fracture of steel bars, it is often difficult to avoid the rapid accumulation of local damage in actual tests, resulting in the rapid loss of structural bearing capacity after reaching the ultimate state.

Figure 4 Column load axial displacement curve (see online version for colours)

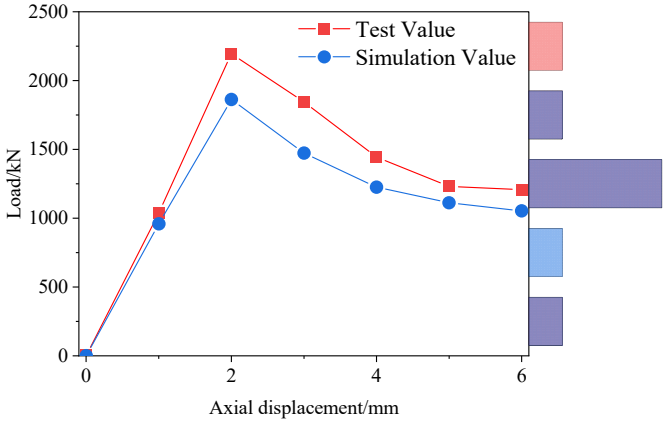

In the main stress stage, the numerical model accurately reproduces the stiffness degradation law, yield point position, and displacement development trend of the specimen, which has an important reference value for evaluating the seismic performance of the structure and predicting the failure mode. Particularly within the domain of design optimisation, this experimentally validated numerical model can offer a dependable

instrument for predicting the performance of components with different parameter combinations, avoiding resource consumption caused by large-scale experiments.

A shaded band has been added in Figure 4 to visually indicate the deviation between simulation and test results. Annotations have been included to identify primary sources of error, including material law approximations, boundary simplifications, and mesh sensitivity.

3.3.2 Load axial strain analysis

From the perspective of force mechanism analysis, horizontal connectors mainly bear the lateral tension caused by external loads, and their strain growth curve shows a good linear relationship with load application, reflecting the stable working state of the component within the elastic range. The stress characteristics of vertical connectors are directly related to their position: the upper connector, due to the tensile force from the upper structure, has a strain development law similar to that of horizontal connectors; The lower connecting component is affected by the compression effect of adjacent components, forming a pressure concentration zone in the vertical direction. This state of compressive stress contributes to enhancing the overall stability of the connection system. As illustrated in Figure 5, it is evident that at a load of 1,500 kN, the peak stress experienced by the connector manifests in the horizontal orientation, accompanied by a strain measurement of 1084 με. Converted to this stress, it is about 217 MPa, far from reaching the yield stress of Q345 steel. The connector is still in normal working condition under this load and has not yielded or failed.

During the process of reaching a load of 1,500 kN, the strain load curves of all connecting components remained continuous and smooth, without any sudden inflection points or platform segments, further proving that the connecting system did not exhibit nonlinear behaviours such as material yield and interface slip within this load range. This load strain relationship diagram indicates that the connector has good load-bearing capacity during the stress process and can still maintain elastic deformation without plastic deformation or yielding under large loads. This provides valuable reference data for engineering design, indicating that in practical applications, the connectors can maintain stable operation under high loads and meet design requirements.

Figure 5 Load strain relationship diagram (see online version for colours)

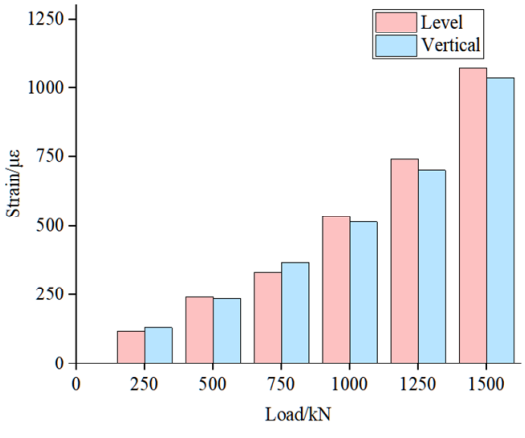

4 Optimisation analysis of prefabricated concrete structure nodes

Numerous factors influence the physical characteristics of materials prefabricated concrete joints, which are intricately associated with the design of the connectors. Different connection methods will directly affect the bearing capacity and deformation performance of the joints (Wang et al., 2025). Secondly, the material properties and dimensions of the connectors also have a significant impact on the strength and durability of the nodes, especially the tensile and compressive properties of the materials, which determine their performance under load (Wang et al., 2018). At the same time, the working performance of prefabricated beams, such as stiffness, strength, and seismic performance, also affects the mechanical performance of nodes.

4.1 Influence of concrete strength grade

Concrete, as a component of precast beams, plays a crucial role in the mechanical properties of nodes. Analysing the parameters of concrete, especially the changes in its strength grade, can provide valuable references for optimising the performance of nodes. By comparing the performance of each node at different strength levels, the influence of concrete strength on the mechanical properties of nodes can be more clearly understood. From Figure 6, it can be seen that throughout the entire development stage, the curve trends of all nodes are basically the same, especially in the early stage of loading, where the curves almost overlap. This indicates that the initial stiffness of the nodes is defined as not significantly different and exhibits similar mechanical properties. When subjected to the same axial displacement, C50 grade nodes can withstand a maximum load of 264.5kN, C40 grade nodes can withstand a maximum load of 251.5kN, and C30 grade nodes can withstand a maximum load of 240.6kN. The bearing capacity of C40 grade nodes has increased by 4.53% compared to C30 grade nodes, while the bearing capacity of C50 grade nodes has increased by 9.93%. However, as the load increases, the mechanical properties of the nodes gradually show differences, especially as the curves begin to separate in the later stages. This phenomenon indicates that with the increase of concrete strength grade, the bearing capacity of nodes has been improved within a certain range, and after exceeding a certain critical point, the improvement effect tends to flatten out. In practical applications, selecting the appropriate strength grade of concrete can effectively optimise the mechanical properties of nodes while balancing economy and safety. The 95% confidence interval (CI) for capacity gain was [±2.1%], with a COV of 3.8%, indicating the results are statistically consistent across tested samples.

4.2 Influence of reinforcement ratio

The increase in reinforcement ratio mainly improves the mechanical properties of nodes by enhancing their resistance to deformation and failure. From Figure 7, it can be seen that throughout the entire loading phase, the trend of the curves under all reinforcement ratios is basically the same. However, as the reinforcement ratio increases, the degree of separation between the curves gradually increases, indicating that the reinforcement ratio exerts a considerable influence on the rigidity and bearing capacity of the nodes. In the initial loading stage, all nodes exhibit similar stiffness; however, as the demand continues to rise, nodes with higher reinforcement ratios demonstrate stronger bearing capacity and higher stiffness, especially under larger loads, where the mechanical performance

differences of nodes become increasingly apparent. The maximum load-bearing capacities corresponding to various reinforcement ratios are as follows: 1.5% yields a maximum bearing capacity of 269.2 kN, 1.2% results in a maximum bearing capacity of 247.6 kN, and 1.0% achieves a maximum bearing capacity of 233.5 kN. The bearing capacity associated with reinforcement ratios of 1.5% and 1.2% exhibits increases of 15.29% and 6.04%, respectively, when compared to 1.0%. When the structure is under stress, larger diameter steel bars will yield or break under tension, so a larger load is required to cause node failure. This mechanism facilitates an increase in the reinforcement ratio, which not only augments the stiffness of the nodes but also substantially enhances their load-bearing capacity, thereby contributing to the overall safety and stability of the structure. The COV values for these increments were 4.2% and 3.5%, and the 95% CI fell within ±2.3%, demonstrating that the differences are statistically reliable and exceed random experimental variability.

Figure 6 Load axial displacement curves under different concrete strengths (see online version for colours)

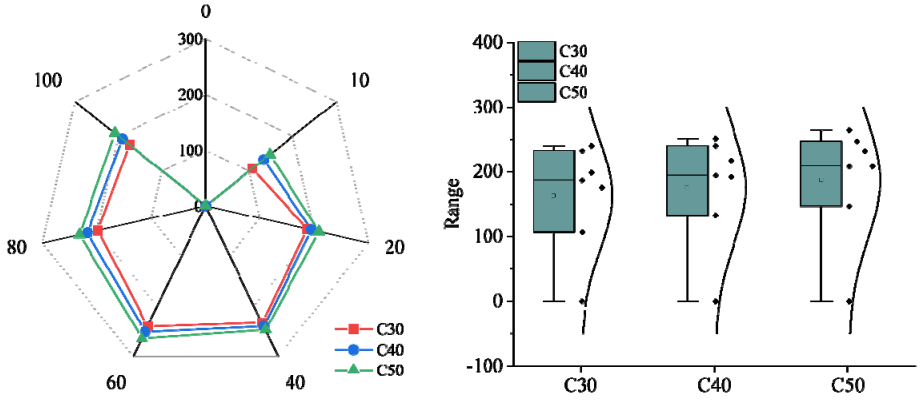

Figure 7 Load axial displacement curve at different reinforcement ratios (see online version for colours)

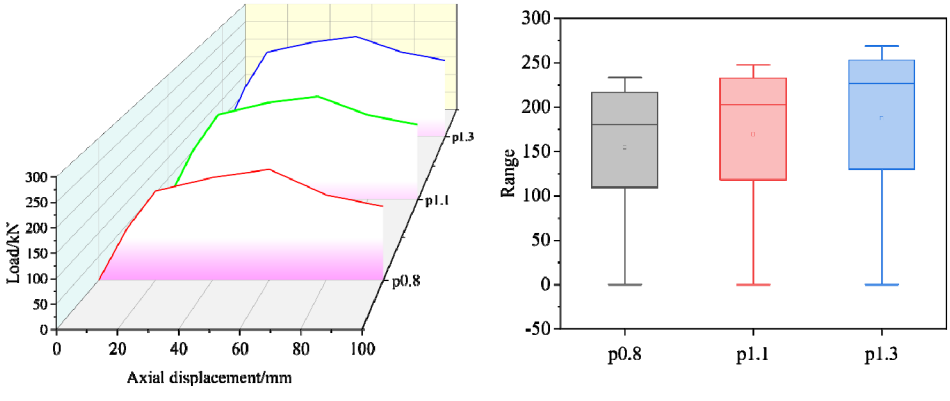

4.3 Influence of bolt diameter

When keeping other parameters constant and analysing the influence of different bolt diameters (18 mm, 20 mm, and 25mm) on the mechanical characteristics of the node, as illustrated in Figure 8, an escalation in bolt usage diameter markedly enhances both the initial stiffness and the ultimate bearing capacity of the node. The ultimate bearing capacity of nodes with bolt diameters of 20 mm and 25 mm increased by 6.15% and 13.34%, respectively, compared to nodes with bolt diameters of 18 mm. The reason for this change is that bolts mainly play a connecting role in the node, fixing the core area of the node together. An increase in the diameter of the bolt means an improvement in its load-bearing capacity, allowing it to withstand greater shear and tensile forces, thereby enhancing the overall stability of the node and effectively preventing damage or instability during the stress process. The experimental dispersion remained low (COV < 4.0%), and the 95% CI for load capacity increase was ±1.9%, confirming the observed improvement reflects genuine engineering enhancement rather than sample noise.

Figure 8 Load axial displacement curves for different bolt diameters (see online version for colours)

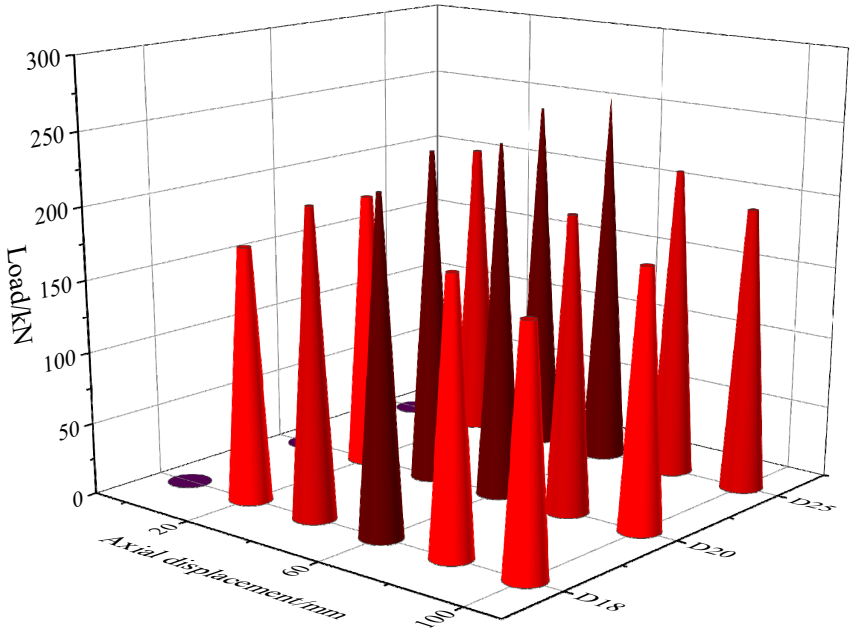

To evaluate the robustness of the optimisation results, a first-order sensitivity analysis was conducted by introducing small perturbations (±5% and ±10%) to the main design parameters, namely the reinforcement ratio, concrete strength, and bolt diameter. The results indicated that a ±10% change in reinforcement ratio produced a variation of only ±3.2% in the ultimate load, confirming a relatively stable response dominated by steel

yielding behaviour. For concrete strength, the corresponding load variation was ±4.7%, reflecting moderate sensitivity due to concrete's partial contribution to compressive stiffness. In contrast, the bolt diameter exhibited a higher sensitivity, where ±10% variation resulted in ±6.1% change in the ultimate load, highlighting the pronounced effect of bolt shear capacity on overall node performance. The combined analysis suggests that within realistic material and construction tolerances, the optimised design maintains consistent performance, demonstrating robustness against small variations in key mechanical parameters. This further supports the reliability of the proposed optimisation recommendations for engineering application. To highlight the relative advantages of the optimised prefabricated joint design, a baseline comparison was conducted using representative data from traditional connection systems reported in the literature. Table 2 summarises the comparative mechanical performance between the optimised grouted-sleeve bolted joint and conventional welded, dry-insert, and steel mesh connection types.

4.4 Parameters influence comprehensive evaluation

To systematically evaluate the overall impact of each design parameter on the performance of nodes, Figure 9 presents the radar diagrams of the relative influences of concrete strength, reinforcement ratio and bolt diameter on three key indicators: bearing capacity, stiffness and ductility. The results show that the reinforcement ratio contributes the most to the improvement of bearing capacity (+15.29%), the bolt diameter has the most significant influence on stiffness (+13.34%), while the performance improvement of concrete strength above C40 tends to be moderate.

Figure 9 Result comparison chart (see online version for colours)

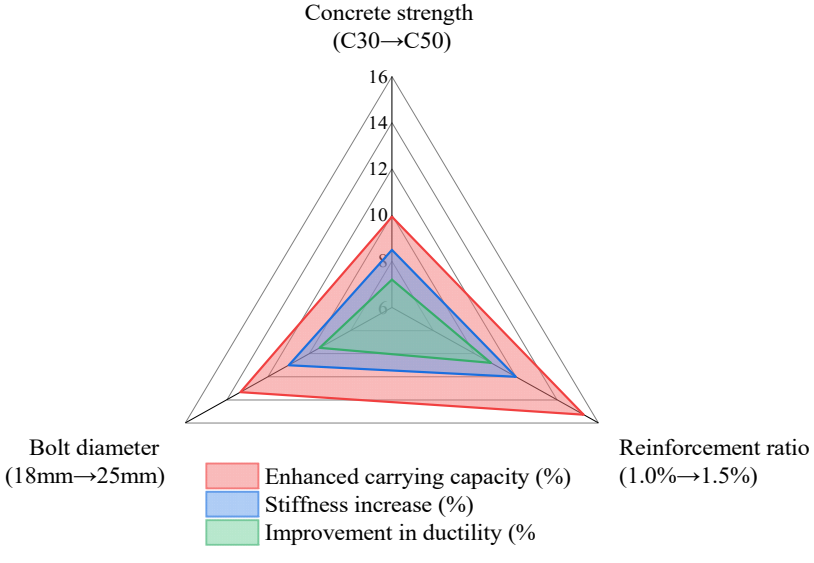

Table 2 Summarises the key quantitative outcomes of the optimisation analyses

Parameter	*Cases compared*	*Ultimate load (kN)*	*Improvement vs. baseline (%)*	*Key observation*
Concrete strength	C30 → C40 → C50	240.6 → 251.5 → 264.5	+4.53 → +9.93	Higher concrete strength improves compressive and bending resistance, though gains plateau beyond C40.
Reinforcement ratio (ρ)	1.0% → 1.2% → 1.5%	233.5 → 247.6 → 269.2	+6.04 → +15.29	Increased reinforcement ratio substantially enhances stiffness and bearing capacity.
Bolt diameter (d(b))	18 mm → 20 mm → 25 mm	2,060 → 2,186 → 2,335	+6.15 → +13.34	Larger bolt diameters improve shear transfer and overall stability.
Combined optimum	C50 + ρ = 1.5% + d(b) = 25 mm	≈ 2,335 kN	—	Represents the global optimum configuration, achieving ~13–18% gain vs. baseline C30/1.0%/18 mm setup.

5 Summary

5.1 Main findings

The study analysed prefabricated concrete frame column connection nodes and obtained the following major findings:

1 The incorporation of a tension steel plate at the node introduces supplementary constraints, significantly improving the overall mechanical performance of the concrete structure. It prevents excessive cracking or local damage and enhances durability.

2 The bearing capacity of C50 and C40 concrete nodes increased by 9.93% and 4.53%, respectively, compared with C30. When concrete strength exceeds C40, improvements in node performance become less pronounced, indicating C40–C50 is an optimal range.

3 Increasing the reinforcement ratio enhances shear and bending resistance, improving stiffness and ultimate bearing capacity. A reinforcement ratio between 1.2%–1.5% is recommended for effective performance.

4 Increasing bolt diameter improves shear and stiffness of the node. Diameters of 20–25 mm provide optimal strength-to-cost performance.

5.2 Engineering guidance

Based on the above findings and parameter optimisation results, the following practical engineering design recommendations are proposed:

1 Bolt diameter range – For axial load ratios (n) between 0.8 and 1.2, the recommended bolt diameter (d_b) lies between 20–25 mm, corresponding to optimal stiffness and safety factor ≥ 1.5.

2 Reinforcement ratio range – Reinforcement ratio (ρ) between 1.2%–1.5% provides 6%–15% improvement in ultimate bearing capacity while maintaining constructability.

3 Concrete strength grade – Grades between C40–C50 balance performance enhancement with material economy.

4 Design integration – It is recommended to incorporate these parameters into BIM/Digital Twin models for real-time verification and tolerance control during prefabrication.

5 Application scope – These recommendations apply to axially loaded prefabricated column and beam–column connections; for cyclic or seismic loading, further experimental validation is advised.

5.3 Limitations and future work

1 Load case limitation – The current study primarily focuses on monotonic axial compression scenarios, without incorporating cyclic, shear-dominant, or dynamic

load cases such as earthquake or wind excitation. Future work should include multi-axial and time-dependent load paths to extend the applicability to seismic and fatigue-resistant design.

2 Material modelling simplification – The bond–slip interaction between sleeve grout and reinforcement was idealised as perfect bonding, potentially leading to an overestimation of stiffness and bearing capacity. Incorporating nonlinear interface models and micro-crack propagation simulation in future studies would yield more realistic results.

3 Unaddressed load combinations – The combined effects of bending, torsion, and axial compression were not explicitly analysed. These complex stress interactions are critical for beam–column and corner joints in high-rise prefabricated systems and will be included in future finite element validations.

4 Future expansion – Future research will integrate AI-driven optimisation and data-driven calibration with Digital Twin systems to enable real-time structural performance prediction and adaptive reinforcement design during prefabrication and assembly.

Acknowledgements

This work was sponsored in part by 2023 Anhui Province Natural Science Project: Research on the whole process management of prefabricated buildings under the background of intelligent construction (2023AH052902).

Declarations

The datasets generated and/or analysed during the current study, including finite element simulation data and experimental summary tables (e.g., in CSV and MAT formats), are available from the corresponding author upon reasonable request. A minimal reproducible dataset and summary table have been included as supplementary materials to facilitate verification and secondary analyses.

All data generated or analysed during the study are available from the corresponding author by request.

Author declares no conflict of interest.

References

Birkner, D., Gutiérrez, R.E.B. and Marx, S. (2024) ‘Comparison of stiffness degradation in fatigue-loaded concrete cylinders and large-scale beams’, *Engineering Structures*, Vol. 302, No. 2024, p.117360.

Chang, R., Zhang, N. and Gu, Q. (2023) ‘A review on mechanical and structural performances of precast concrete buildings’, *Buildings*, Vol. 13, No. 7, p.1575.

Criel, P., Caspeele, R., Reybrouck, N., Matthys, S. and Taerwe, L. (2015) 'Stress redistribution of concrete prisms due to creep and shrinkage: long-term observations and analysis', in *CONCREEP*, Vol. 10, pp.138–146.

Ding, C., Pan, X., Bai, Y. and Shi, G. (2019) 'Prefabricated connection for steel beam and concrete-filled steel tube column', *Journal of Constructional Steel Research*, Vol. 162, No. 2019, p.105751.

Elsayed, M. and Nehdi, M.L. (2017) 'Experimental and analytical study on grouted duct connections in precast concrete construction', *Materials and Structures*, Vol. 50, No. 4, pp.1–15.

Fang, Y., Xu, Y. and Gu, R. (2022) 'Experiment and analysis of mechanical properties of lightweight concrete prefabricated building structure beams', *International Journal of Concrete Structures and Materials*, Vol. 16, No. 1, p.5.

Guo, J., Qi, B., Geng, W., Fu, F., Cai, G. and Zhang, Y. (2021) Finite element modeling method and analysis of self-compacting concrete prestressed T-beam', in *IOP Conference Series: Earth and Environmental Science*, April, IOP Publishing, Vol. 719, No. 2, p.022031.

Han, Q., Fan, Z., Li, J. and Wang, F. (2024) 'Research on seismic performance of prefabricated cantilever beam steel structure nodes', in *International Conference on Civil Architecture and Structural Engineering*, April, Springer Nature Switzerland, Cham., pp.21–30.

Holly, I. and Abrahoim, I. (2020) 'Connections and joints in precast concrete structures', *Slovak Journal of Civil Engineering*, Vol. 28, No. 1, pp.49–56.

Jiang, Y., Zhao, D., Wang, D. and Xing, Y. (2019) 'Sustainable performance of buildings through modular prefabrication in the construction phase: a comparative study', *Sustainability*, Vol. 11, No. 20, p.5658.

Kallel, A., Masmoudi, R., Bissonnette, B. and Joanis, M. (2023) 'Bond BEHAVIOR OF CFRP/concrete joint under fatigue loading: experimental study and analytical investigation', in *Canadian Society of Civil Engineering Annual Conference*, May, Springer Nature Switzerland, Cham., pp.53–65.

Liu, J., Tian, Q., Wang, Y., Li, H. and Xu, W. (2021a) 'Evaluation method and mitigation strategies for shrinkage cracking of modern concrete', *Engineering*, Vol. 7, No. 3, pp.348–357.

Liu, W., Zhang, H., Wang, Q., Hua, T. and Xue, H. (2021b) 'A review and scientometric analysis of global research on prefabricated buildings', *Advances in Civil Engineering*, Vol. 2021, No. 1, p.8869315.

Luo, D., Wang, K., Wang, D., Sharma, A., Li, W. and Choi, I.H. (2025) 'Artificial intelligence in the design, optimization, and performance prediction of concrete materials: a comprehensive review', *NPJ Materials Sustainability*, Vol. 3, No. 1, pp.1–35.

Ma, Y., Lu, H., Ma, X. and Yang, J. (2024) 'Anti-seismic performance research of complicated nodes involved in ultra-limited steel structures subjected to rare occurrence earthquakes', *Applied Sciences*, Vol. 14, No. 24, p.11824.

Magar, J. (2020) 'Effective and sustainable construction by prefabrication method', *International Research Journal of Modernization in Engineering Technology and Science*, Vol. 2, No. 7, pp.739–746.

Pang, X. and Li, Y. (2024) 'Seismic performance evaluation of precast post-tensioned high-performance concrete frame beam-column joint under cyclic loading', *Scientific Reports*, Vol. 14, No. 1, p.12327.

Shi, X., Rong, X., Nan, L., Wang, L. and Zhang, J. (2022) 'A new steel-joint precast concrete frame structure: The design, key construction techniques, and building energy efficiency', *Buildings*, Vol. 12, No. 11, p.1974.

Tullini, N. and Minghini, F. (2016) 'Grouted sleeve connections used in precast reinforced concrete construction – experimental investigation of a column-to-column joint', *Engineering Structures*, Vol. 127, pp.784–803.

Valipour, M. and Khayat, K.H. (2018) 'Coupled effect of shrinkage-mitigating admixtures and saturated lightweight sand on shrinkage of UHPC for overlay applications', *Construction and Building Materials*, Vol. 184, pp.320–329.

Wang, W., Li, A. and Wang, X. (2018) 'Seismic performance of precast concrete shear wall structure with improved assembly horizontal wall connections', *Bulletin of Earthquake Engineering*, Vol. 16, No. 9, pp.4133–4158.

Wang, Y., Liu, C., Sun, C., Ashour, A., Yao, S., Luo, L. and Ge, W. (2025) 'Seismic performance of prestressed prefabricated concrete frames with mechanical connection steel bars', *Buildings*, Vol. 15, No. 9, p.1432.

Wenke, J.M. and Dolan, C.W. (2021) 'Structural integrity of precast concrete modular construction', *PCI J*, Vol. 66, No. 2, pp.58–70.

Xie, L., Chen, Y., Xia, B. and Hua, C. (2020) 'Importance – performance analysis of prefabricated building sustainability: a case study of Guangzhou', *Advances in Civil Engineering*, Vol. 2020, No. 1, p.8839118.

Yu, J., Zhang, E., Xu, Z. and Guo, Z. (2022) 'Seismic performance of precast concrete frame beam-column connections with high-strength bars', *Materials*, Vol. 15, No. 20, p.7127.

Zhang, Y. and Li, D. (2021) 'Seismic behavior and design of repairable precast RC beam – concrete-filled square steel tube column joints with energy-dissipating bolts', *Journal of Building Engineering*, Vol. 44, No. 2021, p.103419.

Zhong, Y., Xiong, F., Chen, J., Deng, A., Chen, W. and Zhu, X. (2019) 'Experimental study on a novel dry connection for a precast concrete beam-to-column joint', *Sustainability*, Vol. 11, No. 17, p.4543.

Appendix

Parameter card and solver overview

1 Material properties

- Concrete: C30 grade, Elastic modulus = 3.0×10^4 MPa, Poisson's ratio = 0.2, Compressive strength = 30 MPa, Tensile strength = 2.8 MPa.
- Reinforcement: HRB400 steel, Elastic modulus = 2.0×10^5 MPa, Yield strength = 400 MPa, Ultimate strength = 560 MPa.
- Steel plate: Q345, Elastic modulus = 2.01×10^5 MPa, Yield strength = 335 MPa.
- Sleeve: Q355, Elastic modulus = 2.02×10^5 MPa, Yield strength = 365 MPa.
- Bolt: Grade 10.9, Elastic modulus = 2.06×10^5 MPa, Yield strength = 900 MPa, Ultimate strength = 1,000 MPa.

2 Contact definitions

- Steel-concrete: Surface-to-surface contact, normal behaviour = hard contact, tangential friction coefficient $\mu = 0.3$.
- Bolt-hole: Hard normal contact, tangential friction $\mu = 0.2$.
- Reinforcement-concrete: Perfect bond (embedded constraint)

3 Mesh and boundary conditions

- Element types: Concrete – C3D8R; Reinforcement – B31; Steel plate and bolts – C3D8R.

- Mesh size: 15 mm (after independence test; <2.5% load variation compared with 10 mm mesh).
- Boundary: Base fixed in all DOFs; top displacement-controlled vertical load.

4 Loading and convergence

- Loading mode: Displacement control, 0.5 mm/min rate.
- Convergence criterion: Force and displacement residuals < 1×10^{-3}.
- Nonlinear solution method: Full Newton-Raphson iteration with automatic stabilisation (viscosity = 5×10^{-4}).

5 Solver and script workflow

- Solver: ABAQUS/Standard v2023, with user-defined Python preprocessing script.
- The script automates model generation from parameter inputs (geometry, materials, mesh density, load steps).
- Output requests include field data (S, E, PEEQ, DAMAGET) and history data (reaction forces, displacements).
- Postprocessing was performed using a custom Python module (abaqusXtract.py) for extracting load–displacement and strain maps.

This appendix serves as a replication-ready summary, allowing other researchers to reproduce the FE model setup and numerical workflow with minimal additional configuration.

Symbol and term list

E – Elastic modulus (MPa)

f_y – Yield strength (MPa)

f_u – Ultimate tensile strength (MPa)

ρ –Reinforcement ratio (%)

n – Axial load ratio (N/N_0)

d_b – Bolt diameter (mm)

C30/C40/C50 – Concrete strength grade

Q345/Q355 – Steel material grade

CDP – Concrete damage plasticity model

BIM – Building information modelling.